Please do not adjust margins

Journal Name

ARTICLE

Conductive elastomer composites for fully polymeric, flexible bioelectronics

Received 00th January 20xx,
Accepted 00th January 20xx

DOI: 10.1039/x0xx00000x

www.rsc.org/

Estelle Cuttaz[a,b+], Josef Goding[a+], Catalina Vallejo-Giraldo[a], Ulises Aregueta-Robles[c], Nigel Lovell[c], Diego Ghezzi[b], Rylie A. Green[a*]

Flexible polymeric bioelectronics have the potential to address the limitations of metallic electrode arrays by minimizing the mechanical mismatch at the device-tissue interface for neuroprosthetic applications. This work demonstrates the straightforward fabrication of fully organic electrode arrays based on conductive elastomers (CEs) as a soft, flexible and stretchable electroactive composite material. CEs were designed as hybrids of polyurethane elastomers (PU) and poly(3,4-ethylenedioxythiophene):polystyrene sulfonate (PEDOT:PSS), with the aim of combining the electrical properties of PEDOT:PSS with the mechanical compliance of elastomers. CE composites were fabricated by solvent casting of PEDOT:PSS dispersed in dissolved PU at different conductive polymer (CP) loadings, from 5 wt% to 25 wt%. The formation of PEDOT:PSS networks within the PU matrix and the resultant composite material properties were examined as a function of CP loading. Increased PEDOT:PSS loading was found to result in a more connected network within the PU matrix, resulting in increased conductivity and charge storage capacity. Increased CP loading was also determined to increase the Young's modulus and reduce the strain at failure. Biological assessment of CE composites showed them to mediate ReNcell VM human neural precursor cell adhesion. The increased stiffness of CE films was also found to promote neurite outgrowth. CE sheets were directly laser micromachined into a functional array and shown to deliver biphasic waveforms with comparable voltage transients to Pt arrays in *in vitro* testing.

1. Introduction

Neuroprosthetic devices aim to restore or bypass motor, sensory or cognitive functions that have been lost or damaged as a result of injury or disease. They span a wide range of applications including the perception of sound via cochlear implants[1] providing artificial vision using retinal implants for the blind[2] and modulation of peripheral nerves for applications such as bladder control[3]. These active implantable devices require the use of electrode arrays as key components to interface with the nervous system. The electrodes are in direct communication with the excitable cell population, enabling both nerve stimulation and recording of neural activity. Conventional electrode arrays utilise metals, such as gold, platinum and platinum alloys, to produce both the electrode sites and the interconnecting tracks that communicate with the implanted electronics[4]. While these metal conductors are known to have stability within the biological environment and to be cytocompatible[5] they also have numerous limitations. Firstly, metallic devices display a high stiffness, with a Young's modulus more than six orders of magnitude larger than neural tissues, resulting in a significant mechanical mismatch at the electrode-tissue interface[6]. The resulting fibrotic encapsulation reduces signal intensity and increases the risk of device failure[7]. Movement of the device within tissues, especially those placed within the cortex or peripheral nervous system, can also result in fracture failure of metal connections. This is an increasing problem as devices and hence track sizes are reduced to minimise invasiveness and increase channel counts. Improving device resolution through increasing channel and electrode numbers is also restricted by the low charge injection limit of metals[8]. Flexible and stretchable organic-based bioelectronics have gained interest as one approach to address these limitations.

It has been proposed that both device failure and inflammatory reactions could be reduced by developing a flexible electrode array composed of entirely polymeric materials[9,10]. The major challenge of such stretchable conductors is to develop a stable material displaying high conductivity while retaining elastic properties. Conductive polymers (CPs) are organic conductors that have attracted significant interest due to their unique combination of high charge injection, chemical stability and relative low cost fabrication[11,12]. Polyaniline (PANI), polypyrrole (PPy) and poly(3,4-ethylenedioxythiophene) (PEDOT) are the

[a] Department of Bioengineering, Imperial College London, London, SW7 2BP, United Kingdom
[b] Center for Neuroprosthetics, Ecole Polytechnique Fédérale de Lausanne, Switzerland
[c] Graduate School of Biomedical Engineering, UNSW, Sydney 2052, Australia
+ Co-first authorship
* Corresponding author: rylie.green@imperial.ac.uk
Electronic Supplementary Information (ESI) available: See DOI: 10.1039/x0xx00000x

Please do not adjust margins

Please do not adjust margins

most commonly used CPs for biomedical applications. CPs can be fabricated with a high roughness and a correspondingly large electrochemical surface area (for a given geometric area) that has been shown to enhance charge transfer[13]. Despite these features, CPs have also been reported to be stiff, brittle and friable[14–16]. Composites of CPs and other more elastic polymers have been shown to address limitations with mechanical performance[17,18]. Substrate polymers such as hydrogels or elastomers[17,18] have been used to ameliorate CP mechanical properties. CP-hydrogel hybrids (or conductive hydrogels, CHs) have been shown to be effective in overcoming limitation in CP mechanical properties while maintaining good electrical conductivity to ensure appropriate material performance[9,18,19]. However, processing CHs into functional electrode arrays with appropriate insulation is challenging due to their high hydrophilicity that can enable ionic ingress. In this study, CPs are combined with elastomers to create conductive elastomers (CE) with the aim of obtaining a composite able to maintain the electrical performance of CPs while enabling processing into full electrode arrays using conventional fabrication methods. Additionally, the mechanical elasticity of these materials can address the challenges of brittle fracture in CPs. An additional benefit of CE composites is their capacity to function as a shield for electromagnetic interference (EMI)[20,21]. This property, imparted by the CP component, is expected to enable implant devices such as neuroprosthetics and cardiac pacemakers fabricated from CEs to be compatible with magnetic resonance imaging (MRI)[20,21]. Composites such as those described above may be a critical enabling technology for the next generation of bioelectronic devices.

Several approaches have been investigated to produce CEs, using either polyurethane (PU)[22–31] or polydimethylsiloxane (PDMS)[32–34] as elastomer matrices. PU and PDMS are typical substrates used for these studies as they impart both flexibility and elasticity to CPs. They have also both been used as components of implantable devices, demonstrating good compatibility with many types of tissues[35–37]. Incorporation of CPs within elastomer matrices has been reported as a straightforward method to produce CEs suitable for applications in tissue engineering[24,25,29] and pressure or strain sensor applications[22,23]. Most of these studies produced materials that exhibited a conductivity on the order of 10^{-4} S.cm^{-1}, a level that is insufficient for use as an implantable electrode array material. Seyedin et al.[23] have shown that wet spinning can produce PU/PEDOT:polystyrene sulfonate (PSS) fibers with strain-sensing capabilities. These CE composites were reported to have a much higher conductivity of 25 S.cm^{-1} at a 25 wt% PEDOT:PSS loading. Additionally, Sasaki et al.[25] produced a 40 wt% PU:PEDOT composite film that was laminated onto a hydrogel, with layers integrated by electrochemical growth of additional PEDOT at the interface between the two materials. At a strain of 100%, the resulting hybrid presented with a large conductivity of 120 S.cm^{-1}, however, the resulting structure was not used to create a functional electrode array and brittle fracture of the PEDOT components was reported. Electropolymerization of a CP within an elastomer has also been utilized for fabrication of CEs.[32] Cakmak et al.[32] has studied the synthesis of flexible PDMS/PPy resulting in conductivities of 3.5 and 5.8 S.cm^{-1} for a CP loading of 88 and 92 wt%, respectively. Mechanical characterization of the composites revealed a Young's modulus in the GPa range while the strain to failure was 8.27% for the highest PDMS content, therefore limiting use of this hybrid in soft and flexible bioelectronics. Finally, chemical polymerization of CPs within elastomers[26,33] can be used to create CEs. Broda et al.[26] used *in situ* chemical polymerization of PPy in a PU emulsion, however the conductivity was quite low (2.3×10^{-6} S.cm^{-1}) at a PPy:PU weight ratio of 20 wt% dry basis. Higher conductivity values were produced using more complex methods[34], including design of block copolymers of modified PDMS and PPy to produce materials with a substantial conductivity of 4000 S.cm^{-1}. [34] However, no characterization of the mechanical properties of these block copolymers was made so it is not known if they are suitable for use in flexible bioelectronics. While this latter method would meet the conductivity and charge delivery requirements for use in stimulating bioelectronics, the complex chemistry is time and resource intensive. This limits the application of this sort of CE material for device manufacture. In summary, existing CE technologies have been limited by their low conductivity or by complicated fabrication methods that limit their application to implantable bioelectronics. In this study, the focus was on developing a CE using simple and scalable methods to produce a material that can be used in conventional electrode array fabrication processes.

This study focused on the fabrication of novel organic flexible electrode arrays using a CE fabricated from PU and pre-formed, chemically synthesised PEDOT:PSS. Bulk CEs were fabricated by dispersing PEDOT:PSS into a PU solution at different loadings (5 wt%, 10 wt%, 15 wt%, 20 wt% and 25 wt%). Characterization of the composite material was performed, including the assessment of physico-chemical properties, electrochemical stability, electroactivity, mechanical behaviour and biological performance. The CE sheets were then fabricated into a flexible electrode array using laser micromachining, a technique commonly used for fabrication of planar electrode arrays based on platinum. The CE sheets were used to create the active sites, tracks and contact pads and were insulated using neat elastomer with no conductive components. The electrochemical properties, including charge transfer characteristics, of the flexible arrays were assessed.

2. Experimental

Materials

Unless stated otherwise, all reagents and materials were purchased from Sigma Aldrich. Thermoplastic PU elastomer pellets (Pellethane 2363-80AE Polyurethane Elastomer, Ether Based) was purchased from Velox GmbH.

This journal is © The Royal Society of Chemistry 20xx

Please do not adjust margins

Fabrication of conductive elastomers

PU films were solvent cast from dimethylacetamide (DMAC) solutions containing 5 wt% (w/v) PU. PU was dissolved in DMAC at 60°C for 24 hours prior to the addition of 0.16 wt% (w/v) of lithium perchlorate ($LiClO_4$). PEDOT:PSS was dispersed in the PU solution at loadings of 5 to 25 wt% (in 5 wt% increments) by stirring for 3 days at 60°C. PU-PEDOT:PSS solutions were cast onto glass plates in a vacuum oven (BINDER GmbH) at an initial isotherm of 60°C for 30 hours and prior to a 6 hour isotherm at 80°C to ensure complete removal of DMAC.

Characterization of material properties

Physico-chemical properties. Surface morphologies of CEs were investigated using scanning electron microscopy (SEM) (JEOL JSM-6400). SEM investigations were conducted using secondary electron detectors operating at a 20kV acceleration voltage under high vacuum. SEM images were taken at magnification of 400x. Energy dispersive x-ray spectroscopy (EDS) (Oxford Instruments INCA) was used to map the chemical composition of CE surfaces, using an electron penetration depth of 7.45 µm[38] for a sheet thickness of 170.00 < t < 208.00 µm. EDS measurements were performed both at the top of the composite and on a cross sectional cut through the film. There were no significant differences found between samples using both methods (cross sectional data not shown). Presence of PEDOT:PSS was assessed by the sulfur content while PU was assessed using nitrogen. A molecular force probe-3D atomic force microscopy (MFP-3D AFM) (Asylum Research, Santa Barbara, CA) was used to acquire topographic images of CE films. Each composite was measured at three different locations. Scan sizes of 10x10 μm^2 were captured at a scan rate of 0.5 Hz. Height maps were flattened and average roughness (R_a) was derived from these processed images using Igor Pro MFP-3D software (Asylum Research, Santa Barbara, CA).

Electrochemical properties. Electrochemical characterization of CE films was comprised of electrochemical impedance spectroscopy (EIS), cyclic voltammetry (CV) and conductivity measurements. EIS and CV were conducted under ambient atmospheric conditions employing a conventional three electrode cell, equipped with a platinum (Pt) counter electrode and an isolated Ag/AgCl reference electrode. Phosphate-buffered saline (PBS) was used as the electrolyte. EIS was investigated by application of sinusoidal voltage between the working and reference electrodes across the frequency range of 0.1 Hz – 10 kHz. CV was evaluated by sweeping the voltage between -0.6V to 0.8V at a 0.15 $V.s^{-1}$ scan rate and the current response was measured. Eleven cycles were performed, and the last cycle was kept for subsequent analysis. The charge storage capacity (CSC) was computed by integration of the current response with respect to time over the defined potential range. All the measurements were accomplished with an AUTOLAB potentiostat-galvanostat (Multi Autolab/M101, Eco Chemie, Netherlands) and the corresponding software Nova 2.0 enabled to control the parameters of EIS/CV and to record the output. Conductivity was assessed by using a two probe set-up. A CE rectangular strip was clamped at each end (using metallic holders) and connected to a potentiostat. The resistance was measured by the two methods EIS and CV. Impedance output from EIS was extracted at 1 kHz while the slope of the resulting CV measurement was computed to derive the resistance. Knowing the geometry of the measured sample, the conductivity (σ) was obtained from the derived resistance values using the following formula (1):

$$\sigma = L / (R \times A) \quad (1)$$

wherein L = length, R = computed resistance, A = cross-sectional area of the sample. Results are reported as means over three samples per batch and averaged over three batches.

Mechanical behaviour. Mechanical behaviour was examined by tensile testing with a Bose electroforce 3200 (BOSE, USA). Polymer strips of 2.3 x 1 x t cm^3 (t < 240 µm) were cut from bulk samples and clamped to the grips to avoid slippage of the samples. Tensile tests were conducted with a crosshead speed of 0.5 $mm.s^{-1}$ and using a 225-N load cell. The first part of the experiment included a pre-loading of 3 N of each sample, followed by three repetitive loading-unloading cycles of 5% strain. A linear regression was performed on the two last cycles and the obtained slope was used to derive the Young's modulus. Polymer strips were also tested under strain to failure conditions. Analysis of the load-elongation output allowed for evaluation of the stress-strain characteristics, as well as the ultimate tensile strength (UTS) and elongation at fracture.

Cell culture. ReNcell VM human neural precursor (ReN) cells were purchased from Millipore, UK and cultured in ReNcell TM NSC maintenance medium (Millipore, UK) containing 20 $ng.ml^{-1}$ of Epidermal Growth Factor (EGF) (Millipore, UK) and 20 $ng.ml^{-1}$ of Basic Fibroblast Growth Factor (FGF-2) (Millipore, UK). The maintenance cell culture media was changed every three days until the cells were confluent. For neuronal/glial differentiation, the cells were cultured in the absence of growth factors EGF and FGF-2, and media was changed every two days. To control the surface area of culture, the pure PU and the CEs were placed in customized silicone Ace O-rings with wall dimension of 1.78 mm and I.D of 10.80 mm and were sealed around the borders of the surface area with silicone elastomer (Sylgard 184). The materials were placed in six well culture plates and autoclaved for two hours, and subsequently washed repeatedly with Hank's balanced salt solution (HBSS) and incubated overnight at 37°C, 5% CO2 for neural cell culture. Prior to plating, samples and control were coated with Laminin (Sigma, UK). A quantity of 20 000 $cells.cm^{-2}$ was plated on each sample, and then 500 µL of the differentiation medium was added to each well and changed with fresh media every two days for a period of seven days**.**

Immunofluorescent labelling. Indirect double-immunofluorescent labelling was performed to visualize

Please do not adjust margins

neurons and astrocyte cell populations as described by Vallejo-Giraldo et al.[39] Briefly, ReN cells on experimental and control samples were fixed with 4% paraformaldehyde and 1% of sucrose for twenty minutes at room temperature at the experimental end point. Once fixed, the samples were washed with PBS and permeabilized with buffered 0.5% Triton X-100 within a buffered isotonic solution (10.3 g sucrose, 0.292 g NaCl, 0.06 g $MgCl_2$, 0.476 g HEPES buffer, 0.5 ml Triton X-100, in 100 ml water, pH 7.2) at 4°C for five minutes. Non-specific binding sites were blocked with 1% bovine serum albumin (BSA) in PBS at 37°C for 30 minutes and subsequently incubated for two hours with a 1:200 concentration anti-glial fibrillary acidic protein (GFAP) antibody produced in mouse (Sigma, 1:200) and 1:500 concentration anti-β-Tubulin III antibody produced in rabbit (Sigma, 1:500). Samples were washed three times with 0.05% Tween 20/PBS and then incubated for one hour in the secondary antibody Alexa Fluor® 488 goat anti-Mouse IgG / IgA / IgM (H+L) (Molecular probes 1:500) combined with the secondary antibody Alexa Fluor® 594 goat anti-Rabbit IgG (H+L) (Molecular probes, 1:500). Samples were washed with PBS (five minutes ×3) and mounted on microscope cover slides and counterstained with slowfadeR gold antifade reagent with DAPI for nuclear staining.

Microscopy and Image Analysis. After immunostaining, samples were viewed with a Leica SP8 Inverted Confocal Microscope at a fixed scan size of 1024 by 1024 at a ratio 1:1. Cell analysis was performed as described by Vallejo-Giraldo et al.[39] At least twenty images at 63× magnification were taken at random from each experimental group and control. Cell density was analyzed by counting the total number of labelled nuclei corresponding to neurons and astrocytes in an area of 309.78 µm x 309.78 µm. Neurite length was quantified by analyzing nine random fields of view of three different technical replicas using established stereological methods[40]. The formula used was:

$$\text{Neurite length} = N \times T \times \pi/2 \quad (2)$$

where n is the number of times neurites intersect grid lines and T = distance between gridlines (taking magnification into account) as described by Vallejo-Giraldo et al.[39]

Statistical Analysis for Cell Studies. All data presented within was confirmed using at least three replicates for each of the test groups and control group. The results are expressed as the mean of the values ± standard error of the mean, unless otherwise stated. One way ANOVA followed by a Bonferroni test were performed to determine the statistical significance ($p<0.05$), unless otherwise stated.

Fabrication of conductive elastomer arrays

Electrode arrays were fabricated using a protocol previously reported for Pt based implant arrays[41–43], but modified to replace the Pt foil with a CE sheet. Both 10 wt% and 15 wt% PEDOT:PSS in PU were assessed. The insulative material used was poly(dimethyl siloxane) (PDMS) (MED-1000, NuSil, Carpinteria, CA, USA) mixed in a one-to-one ratio with hydrocarbon solvent (n-heptane, Ajax Chemicals Ltd, Sydney, NSW, Australia). The laser electrode fabrication technique employed has been described by Dodds et al. [44]. Briefly, a standard microscope slide was covered with adhesive silicone tape (No. 4124, Tesa® AG, Germany) as a release layer. Then a base layer of n-heptane diluted PDMS (1:1 ratio) was spin coated, as a support substrate. A thickness of 60 µm was achieved using 2000 rpm for 90 s at room temperature (21°C). The layer was cured at 60°C for 15 min. The CE sheet was applied to the slide and the electrode array configuration was patterned onto the CE using a numerically controlled laser (Nd:YAG, Firescan DPL Genesis Marker, CAB GmbH, Karlsruhe, Germany). Waste materials were removed manually and a second layer of PDMS/n-heptane was applied using identical process parameters to fully insulate the CE array. Finally, the contacts pads and electrodes were opened by a two-step process of first laser crystallising (Excimer Laser, Atlex 300 SI, Germany) and then ablating the overlying PDMS.

In vitro charge transfer characteristics

The potential transient response was measured in a three-

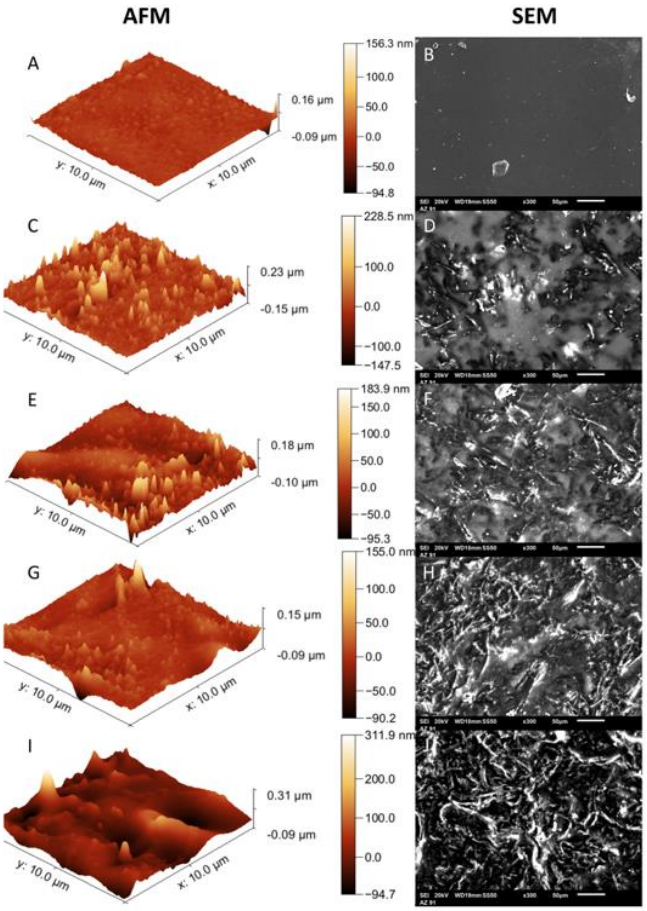

Fig. 1 AFM (left) and SEM (right) images of CE surface. 3D AFM maps of (a) pure PU, CEs at a loading of (c) 5 wt%, (e) 10 wt%, (g) 15 wt% and (i) 20 wt%. SEM images at 300x magnification of (b) pure PU, and CEs at a loading of (d) 5 wt%, (f) 10 wt%, (h) 15 wt% and (j) 20 wt%.

This journal is © The Royal Society of Chemistry 20xx

Please do not adjust margins

Please do not adjust margins

electrode system with an isolated Ag/AgCl reference electrode, low impedance Pt counter electrode and the test electrode immersed in PBS. Current controlled biphasic waveforms were applied to determine the charge injection limit. The maximum negative potential excursion (E_m) in the voltage transient is used to determine this limit. This metric has been previously described by Cogan et al[45]. E_m was calculated by subtracting the access voltage (V_a), associated with the ohmic resistance of the system. E_m was measured to include the interpulse potential (IPP) following the delivery of the first phase of the stimulus. An interpulse delay of 0.02 ms was applied to increase the accuracy of the measurement. The electrochemical charge injection limit (CIL) was defined as the quantity of the charge that polarizes the electrode interface to the potential for water reduction (E_m = -0.6 V vs Ag/AgCl). The pulses were applied cathodic first, as is common practice for implant stimulations. The phase length was set at 0.2 ms and the current was increased to obtain the limit. Sample biphasic waveforms below the electrochemical CIL were obtained at 200 µA amplitude and 200 µs phase length to better understand the charge transfer mechanisms within the array.

Statistical analysis

Data were analysed using Matlab software (The Mathworks Inc., USA) and Excel (Microsoft, USA) and was reported as the mean ± standard deviation (SD). One way or two-way ANOVA was applied as indicated, followed by Tukey post hoc tests for multiple comparisons. Statistical significance was considered when $p < 0.05$.

3. Results and discussion

CEs were fabricated with varying PEDOT:PSS content with 5 wt%, 10 wt%, 15 wt%, 20 wt% and 25 wt% loadings. CEs appeared as dark-blue sheets, becoming more opaque and darker as the PEDOT:PSS loadings increased. CE composites with 25 wt% PEDOT:PSS loadings were excluded from some tests after electrochemical analysis revealed no benefit in electrochemical properties when exceeding 20 wt% PEDOT:PSS content. While the volume used to cast the CE was constant across all formulations, the thickness of the CE sheets ranged from 170.00±14.81 µm to 209.33±13.38 µm (Table 1). It was noted that the thickness increased in line with higher PEDOT loading.

CE bulk properties

Fig. 1 displays the surface-based physico-chemical characterization of the CEs as assessed by SEM-EDS and AFM. Increased loadings of PEDOT:PSS saw the evolution of rough surface topographies compared to the more flattened surface exhibited by the pure PU (Fig. 1). This was supported by the computation of the average roughness from AFM results. Table 1 exhibits the increase in R_a observed in CEs as the content of PEDOT:PSS embedded in the PU matrix increased, ranging from 4.59 ± 1.17 nm for pure PU to 52.29 ± 21.34 nm for 20 wt% PEDOT:PSS/PU composite. The morphological changes suggested by R_a analysis were also observed, as seen in Fig. 1. The SEM micrographs of CEs exhibited entangled rod-shaped structures in the surface. At the lowest PEDOT:PSS content, a random organization can be noticed compared to the flatness of the pure PU profile. The gradual increase in PEDOT:PSS in the CEs showed an evolution towards a more connected organization. SEM-EDS chemical analysis highlights the uniformity of dispersion obtained when combing these two polymers, as shown on Fig. 2. EDS elemental analysis of sulfur and nitrogen both showed a homogeneous distribution for all PEDOT:PSS/PU composites at lower PEDOT loadings (< 15 wt%). Overlay of the elemental nitrogen and sulfur maps onto the corresponding SEM pictures implied a uniform distribution of sulfur among the nitrogen atoms, suggesting that generally well-dispersed polymer composites were obtained. At higher loadings (15 wt% and 20 wt%), rod-shaped areas of high sulfur content were observed, indicating aggregation of PEDOT:PSS into fibres. Future studies will include thermogravimetric analysis (TGA) of the material to look more thoroughly into component analysis and explore other processing routes.

Table 1 Thickness and AFM surface average roughness (R_a) of pure PU and CEs at a loading of 5 wt%, 10 wt%, 15 wt%, 20 wt% and 25 wt%. Results are reported as mean ± SD (n = 3)

Samples	Thickness [µm]	R_a [nm]
Pure PU	189.33 ± 13.20	4.59 ±1.17
5 wt% CE	170.00 ± 14.81	18.15 ±8.91
10 wt% CE	176.67 ± 12.32	33.60 ±14.61
15 wt% CE	197.33 ± 14.61	35.10 ±27.65
20 wt% CE	208.00 ± 11.72	52.29 ±21.34
25 wt% CE	209.33 ± 13.38	-

Electrical performance of CE was investigated by EIS, CV and conductivity measurements. Bode plots of the impedance magnitude and phase angle of the PEDOT:PSS/PU composites are depicted in Fig. 3A and 3B respectively. The impedance magnitude was found to decrease with increasing PEDOT:PSS content over the 1 - 10 kHz frequency range. A significant decline of impedance and increase in conductivity was noticed between the 5 wt% and 10 wt% PEDOT:PSS/PU composites, suggesting that some percolation threshold was crossed between these two loadings. No reduction in impedance was observed as PEDOT loading was increased from 20 wt% to 25 wt%, suggesting a saturated PEDOT:PSS network. At low frequency, CEs with a PEDOT:PSS content above 10 wt% displayed a significant reduction in impedance magnitude of

Please do not adjust margins

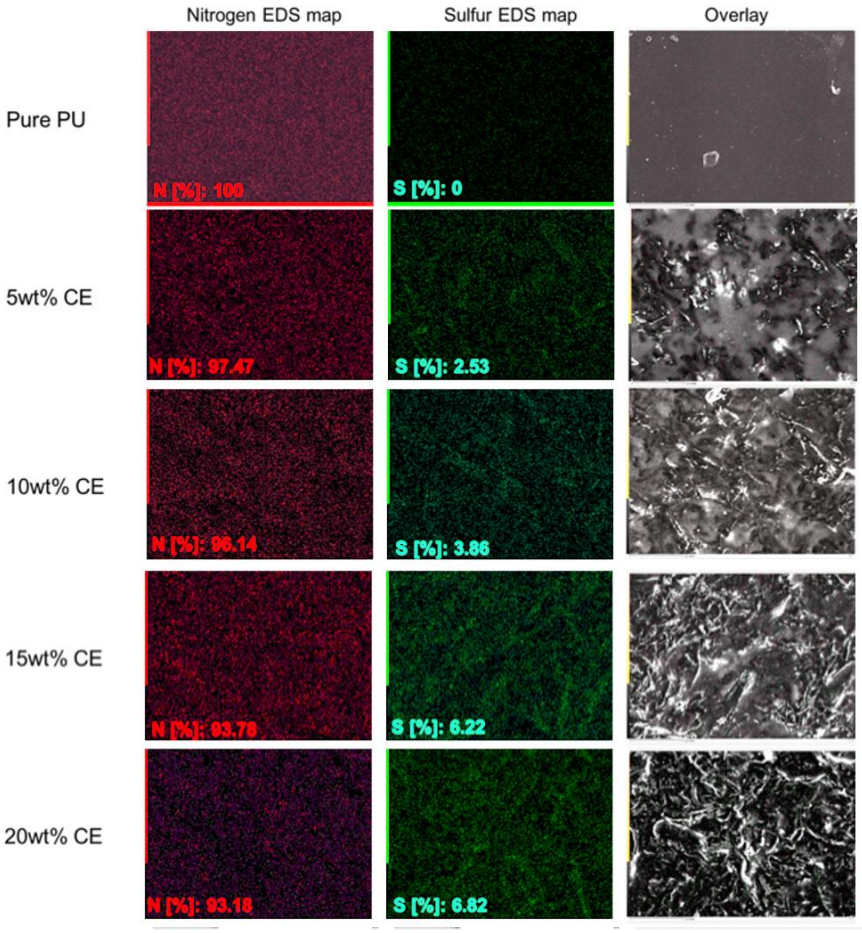

Fig. 2 SEM-EDS analysis of pure PU and PEDOT:PSS/PU composites. Each block displays the EDS elemental mapping of Nitrogen and Sulfur with the corresponding relative mass components of PU and PEDOT respectively. The third column shows the SEM topography, demonstrating the relationship between topography and distribution of PEDOT:PSS in CE composites as a function of PEDOT:PSS loading.

more than one order of magnitude compared to platinum. All CE composites had impedance magnitudes above platinum at 1kHz, the characteristic biological frequency (see Table 2) and above 1kHz. The phase angle of all CE composites indicates they preferentially transfer charge using faradaic mechanisms.

Table 2 Impedance at 1kHz of Pt and CEs at a loafing of 5 wt% , 10 wt%, 15 wt%, 20 wt% and 25 wt%. Results are reported as mean ± SD (N = 3)

Samples	Impedance at 1kHz [Ohm.cm^2]
Pt	7.51 ± 1.63
5 wt% CE	143.32 ± 42.14
10 wt% CE	31.70 ± 5.46
15 wt% CE	19.97 ± 3.52
20 wt% CE	14.80 ± 3.85
25 wt% CE	13.59 ± 4.30

The cyclic voltammograms of the CE at different PEDOT:PSS contents are displayed in Fig. 3C. The trapezoid shape of CV exhibited by each kind of CEs showed evidences of both capacitive and resistive charge transfer, highlighting the pseudo-capacitive behaviour of the CEs. Regarding the impact of CP loading, larger histograms were observed with increasing PEDOT:PSS loadings. This trend was quantified by CSC computation, as shown in Figure 3D. It was observed that incorporation of an increasing amount of PEDOT:PSS into PU led to a linear gain in the CSC, with for example, CSCs of 63.99 ± 4.47 and 94.59 ± 9.02 mA.cm^{-2} for 10 wt% and 15 wt% CE, respectively. It should also be noted that 5wt% and 25 wt% PEDOT:PSS/PU composites exhibited CSC values one and two orders of magnitude larger that of Pt, respectively. One way ANOVA suggested significant differences between CE's of different loadings ($p = 6.0694e-6$). Tukey's post hoc test revealed that there was no statistical significant difference in CSC between the 20 wt% and 25 wt% PEDOT:PSS/PU composites ($p= 0.2441$). These findings confirm that CEs demonstrate a significant benefit in electrochemical performance over conventional Pt electrodes. Improvement of electrochemical characteristics could be explained by the rough

This journal is © The Royal Society of Chemistry 20xx

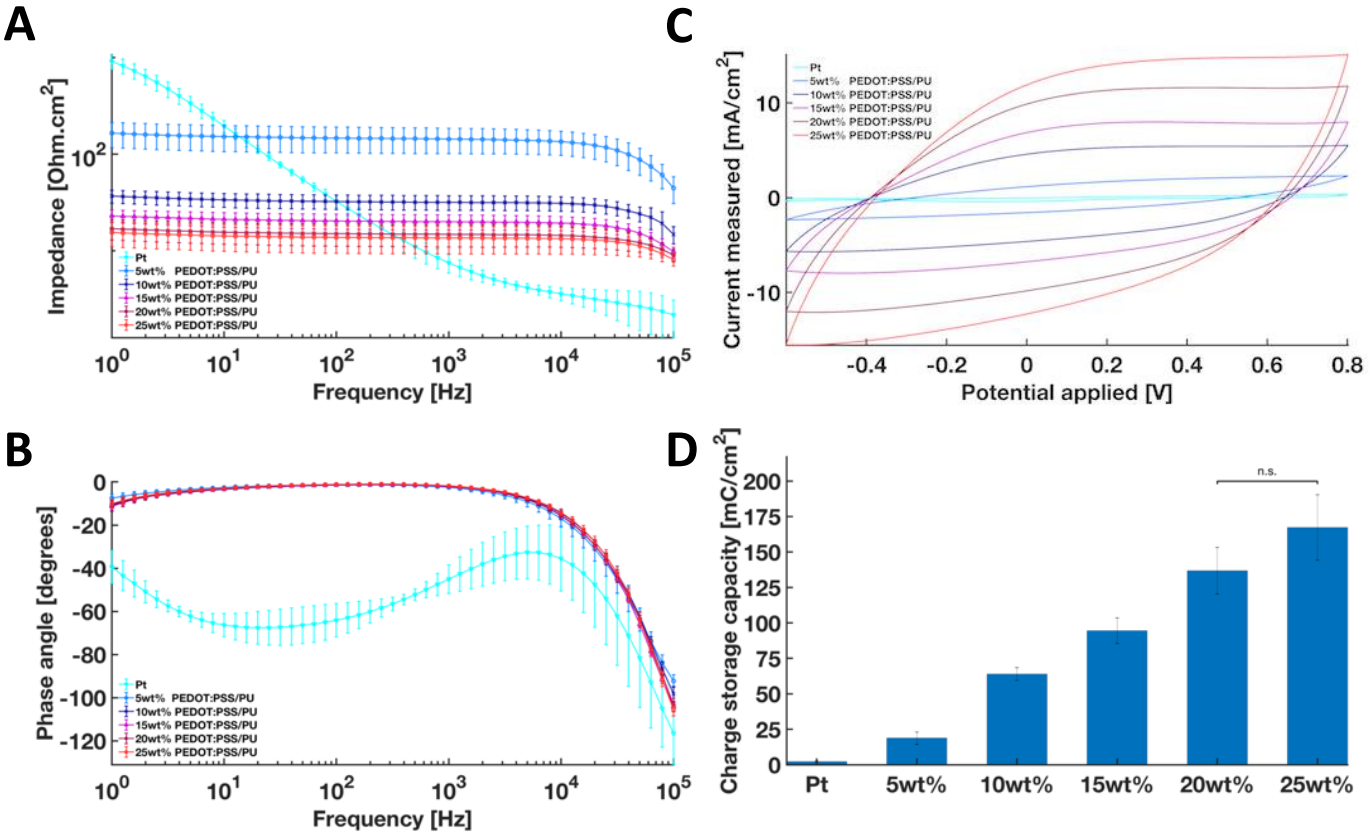

Fig. 3 A) Impedance magnitude and B) Phase angle of PEDOT:PSS/PU composites at varying PEDOT:PSS loadings. C) Cyclic voltammograms and D) charge storage capacity of CE composites with varying PEDOT:PSS loadings. Data represent the mean± standard deviation (average across three different batches, n = 5). One way ANOVA followed by Tukey post hoc test was run. * Significant difference at $p < 0.05$.

surface of CEs as observed previously in the AFM analysis. This roughness could increase the interfacial surface area available for charge transfer, which results in lower impedance and higher capacitance, thereby enhancing the electrochemical performance. This may also be a result of the mixed charge transfer mechanisms exhibited by PEDOT-based materials as described above. Fig. 4 shows the conductivity versus PEDOT:PSS loadings obtained by two different methods, EIS at 1kHz and CV. The electrical conductivity increased linearly with additional incorporation of CP, suggesting the formation of a conductive network of PEDOT:PSS within the PU elastomer. Additional conducting paths are created by the further integration of PEDOT:PSS, resulting in enhanced electrical performance. Conductivity investigated with EIS at 1kHz resulted in a range from 0.25 ± 0.07 $S.cm^{-1}$ at the lowest loading to 6.59 ± 0.62 $S.cm^{-1}$, achieved at 20 wt%. Regarding the CV results, the lowest conductivity was 0.31 ± 0.07 $S.cm^{-1}$, which occurred at 5 wt% while the highest conductivity was 7.13 ± 0.44 $S.cm^{-1}$ for a PEDOT:PSS ratio of 20 wt%. This could imply that there is no benefit in increasing the PEDOT:PSS content from 20 wt% to 25 wt%, phenomena already evidenced in the impedance and CSC analysis. Statistical analysis showed that the results differed between the two methods of determining conductivity for each type of CE and between each loading (two-way ANOVA, $p = 0$ and $p = 0.041$ respectively). Overall CEs possess a conductivity falling in the range of the semi-conductors[17]. Some research groups[23,27] have obtained higher conductivities for similar composite materials. For example Seyedin et al.[23] produced PU/PEDOT:PSS fiber at a loading of 25 wt% achieving a conductivity of 25 $S.cm^{-1}$. However the 25 wt% PEDOT:PSS composite fibers exhibited a 30-fold increase in the Young's modulus' magnitude compared to pure PU, while only

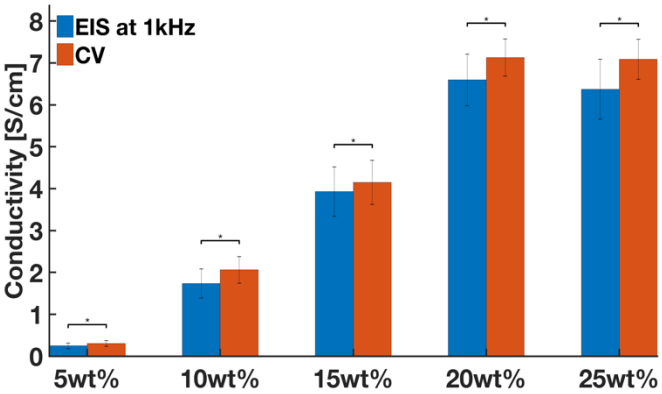

Fig. 4 Conductivity of PEDOT:PSS/PU composites with varying PEDOT:PSS loadings measured in a dry cell with two different methods: EIS at 1kHz (left) and CV (right). Data represent the mean± standard deviation (n = 3). For all loadings across both methods, the differences in conductivities were statistically significant (two way ANOVA, $p = 0.041$). * Significant difference at $p < 0.05$.

Please do not adjust margins

a 10-fold reinforcement in elastic modulus was obtained in this work for the same CP content increase (see Section Mechanical Behaviour). However, literature also reports lower conductivity values when mixing PU with other CPs [17,24,30,31]. For example, thermoplastic PU/polythiophene derivative (40:60) blends have been produced to form nanomembranes with conductivities ranging from 2.23 x 10^{-5} to 5.19 x 10^{-6} S.cm^{-1} [24].Conductive AFM analysis revealed an irregular dispersion of CPs chains within the PU insulative network, affecting the electrical performance of the composites. Several studies demonstrated conductivities below 10^{-4} S.cm^{-1}, where the maximum CP loadings reached was inferior to 12 wt%[30,31]. Another possible factor in the conductivity of CE composites is the excess PSS present in dispersible PEDOT:PSS. The presence of excess PSS has been demonstrated to restrict the conductivity of PEDOT:PSS cast films, an effect which can be reversed by solvent washes designed to remove excess PSS [46]. The solvent-based processing used within this study may have facilitated the re-arrangement of excess PSS and possible dopant exchange with the $LiClO_4$ ions used to aid the dissolution of PU. Both of these processes may contribute to the relatively high level of conductivity observed in the PEDOT:PSS/PU composites. Mechanical behaviour of the CEs evaluated by tensile tests was greatly affected by incorporation of PEDOT:PSS within PU (Fig. 5). Representative stress-strain curves of pure PU and CE composites are displayed in Fig. 5A. Pure PU possesses a non-linear visco-elastic behaviour, coming from its characteristic structure composed of soft and hard segments domains, whereby the soft segments impart elastic properties while the hard segments provide the physical crosslinks[47]. A significant loss of elastomeric properties proportional to the PEDOT:PSS weight ratio was observed. As a larger amount of PEDOT:PSS was incorporated into PU, the slope of the initial stiff region tended to increase while the following compliant behaviour became shorter, resulting in an earlier fracture compared to pure PU. Indeed as depicted in Fig. 5B, a substantial elongation at failure of 346 % was reached for 5 wt% PEDOT:PSS/PU composites, which subsequently linearly decreased as more CP was added, to obtain a 25 wt% CE capable of 134% extension at failure. Even though this 3-fold decline in extension is significant, achieving outstanding elongation at failure is not necessary for biomedical applications, as the maximum strain at

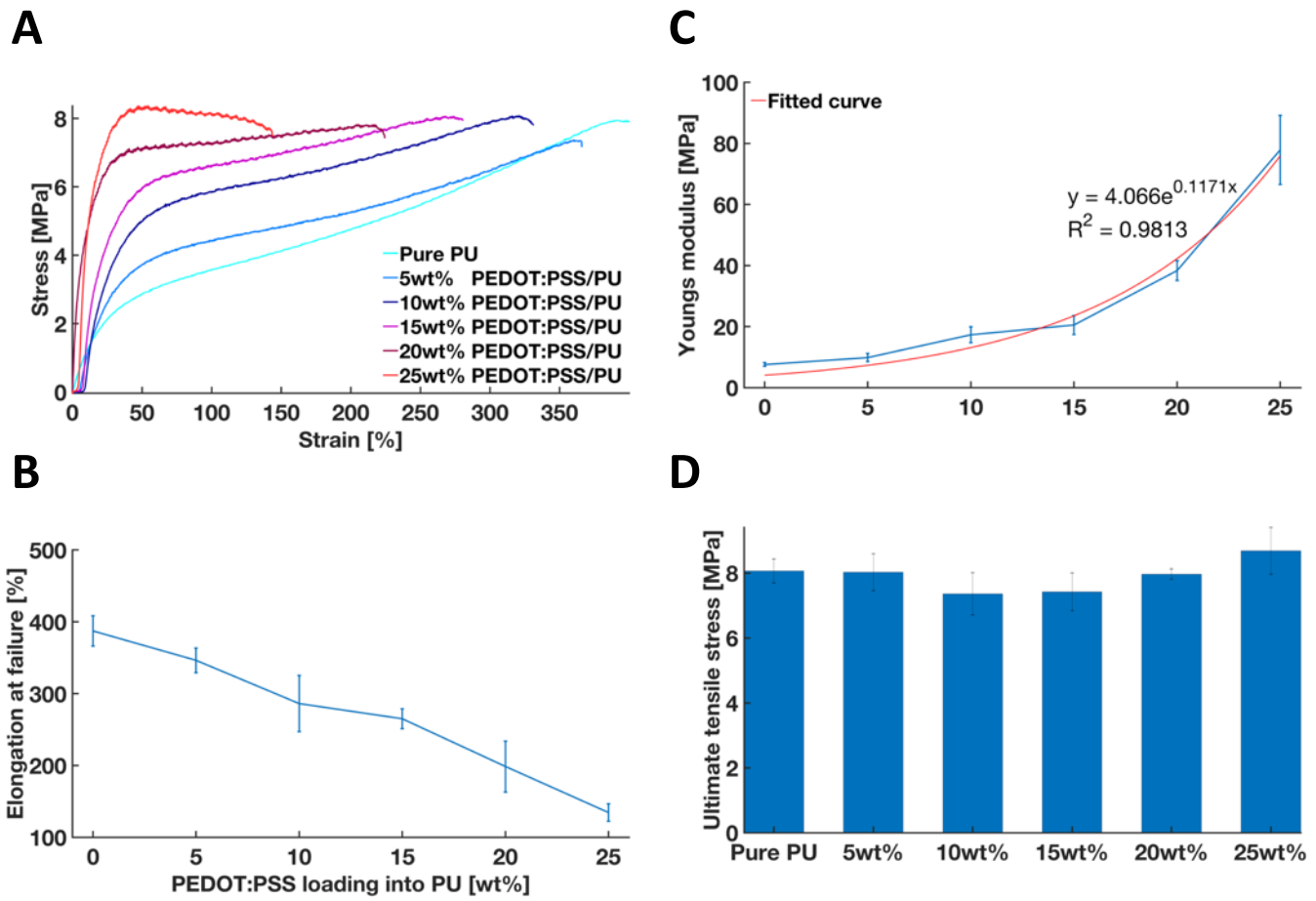

Fig. 5 Mechanical properties of PEDOT:PSS/PU composites at different PEDOT:PSS loadings. A) Representative tensile stress-strain curves B) Elongation at failure C) Young's modulus and D) Ultimate tensile strength. One way ANOVA revealed that there were no statistically significant differences between UTS group means. Data represent the mean ± standard deviation (n = 3). * Significant difference at $p < 0.05$.

This journal is © The Royal Society of Chemistry 20xx

Please do not adjust margins

fracture experienced in the brain is around 20%[48]. Therefore, the obtained elongations at failure are sufficient for biomaterial applications. Furthermore, at a strain of 20% the CE composites are still operating within their elastic region. The Young's modulus was exponentially increased from 9.85 ± 1.33 MPa, a value close to pure PU (7.57 ± 0.58 MPa), to 77.88 ± 11.30 MPa when increasing the loading from 5 wt% to 25 wt% (Fig. 5C). A study from Seyedin et al.[23] has showed a similar behaviour for the Young's modulus and the elongation at failure. However Seyedin et al.[23] reported lesser impact on mechanical properties at low PEDOT:PSS loadings (i.e. lower Young's modulus and higher elongation until fracture), but this tendency reversed at higher PEDOT:PSS amounts (i.e. 20 wt% and 25 wt%), where the Young's modulus is in excess of 100 MPa and strain to failure fell below 100%. Broda et al.[26] also obtained an increasing material stiffness as the mass ratio of CP to PU increased. The microscopic mechanisms underlying this elastic modulus enhancement might be explained by the hydrodynamic strain amplification effect, where the addition of relatively more rigid fillers (i.e. PEDOT:PSS) to a soft elastomer matrix leads to local strain amplification[49–51]. Therefore, the resulting composite possesses a combination of the mechanical properties of the rigid filler and elastomer in a CP/PU ratio-dependant fashion. Furthermore, mechanical, physical and chemical interactions between the conductive fillers and PU may also have an effect on this reinforcement[51]. Regarding the tensile strength, Figure 5D shows that the UTS values did not display a pattern dependent on the ratio of PEDOT:PSS/PU, as observed for the ther mechanical parameters. The UTS exhibited steady values around 7-8 MPa for all the loadings, which is in line with the UTS of pure PU. One way ANOVA revealed that the results were found to not statistically differ between each CE and pure PU. These findings differ from reports in the literature, as Seyedin et al.[23] demonstrated a rapid decrease in UTS with increasing PEDOT:PSS fibre loadings in PEDOT:PSS/PU composite. This degradation in tensile strength was attributed to the system's structural heterogeneity as well as to the presence of PEDOT:PSS particles within the elastomer network, which could disrupt the soft segments domains interactions, responsible for the elastomeric properties of the PU[47]. Interestingly, Broda et al.[26] reported a stable UTS among PU/CPs composites produced by in situ polymerization of PPy within a PU emulsion, at lower UTS than pure PU, which is not the case in this work. The observed uniform decrease in UTS was attributed to the biphasic nature of the two-component composites. The introduction of particle fillers resulted in weak bonding between the PPy and PU components, resulting in discontinuities which impair the mechanical integrity of the composite. Another important feature of these CEs is the effect of an applied strain onto their electrical characteristics. Several studies showed that mechanical stretching of PU-CPs composites resulted in changes in conductivity, revealing a piezoresisitve behaviour[23,25,27]. Future studies will explore more thoroughly this effect and the corresponding underlying mechanism by electromechanical tensile testing. Such analysis could give insight into the conductive network morphology and the interaction between PEDOT:PSS and the elastomer matrix.

Biological response

Fig. 6A shows representative micrographs of neuron and astrocyte cell populations cultured on pure PU and the CEs using ReNcell VM human neural precursor (ReN) cells over a period of seven days in culture. CE composites of 10 and 15 wt% were identified as the ideal trade-off between mechanical and electrical properties (large increases in conductivity with only minimal increase in Young's modulus) for fabrication of flexible electrode arrays (see below) and consequently these two composites plus neat PU were chosen for biological assessment. Fig. 6B reveals the neuron cell percentage present in the mixed culture on pure PU and CE composites with no statistical differences among composites but revealing a significance difference between the PU control and the CE composites. The pure PU control showed a neural cell population of 33%, compared to 52% and 53% for the 10 wt% and 15 wt% CEs respectively, indicating greater neuronal survival on CE composites. Figure 6C details the neurite outgrowth of the ReN neural cultures. The average neurite length was shown to significantly decrease from 298.4 ± 16.9 μm on pure PU to 139.2 ± 11.7 μm for 10 wt% CEs, followed by a further significant decrease for 15 wt% CEs with neural length of 45.2 ± 1.5 μm. It is interesting to note that neural survival did notably increase with the increase in nano-roughness associated with higher PEDOT:PSS loadings, while at the same time neurite outgrowth decreased due to the associated increase in Young's modulus.
Cell-substrate interactions are typically governed by complex mechanisms occurring at the nanoscale level[52], furthermore the role of astrocytes in providing a mechanical substrate for the growth of neural cells is well established. [53–55] Favourable roughness for culture of neurons is approximately 32 – 36nm, which helps facilitate adsorption of key serum proteins such as fibronectin and laminin which in turn promote neural adhesion.[56,57] Table 1 shows that both of the CEs evaluated for their biological response, 10 wt% CE and 15 wt% possess roughness values similar to those of the reported favourable range explaining the increase in neural cell population observed for CE composites compared to neat PU. Furthermore, the particular elongation or retraction of the neurites observed on the CEs and control may correspond to the stiffness effect on neurite extension[58–61]. The neurite outgrowth observed on each of these groups highlights the importance of threshold stiffness and the ability of neurons to sense these alterations by changing their neurite outgrowth and elongation[62–65]. Our data suggests that an optimal stiffness range of 8MPa to 17MPa promotes neurite elongation. Of further interest is the observation that the 10 wt% CE shows an interesting promotion of both neuron presence and neurite outgrowth, suggesting that neurons in the presence of an underlying glia network may benefit from a morphological or structural material-composite effect. In turn,

Please do not adjust margins

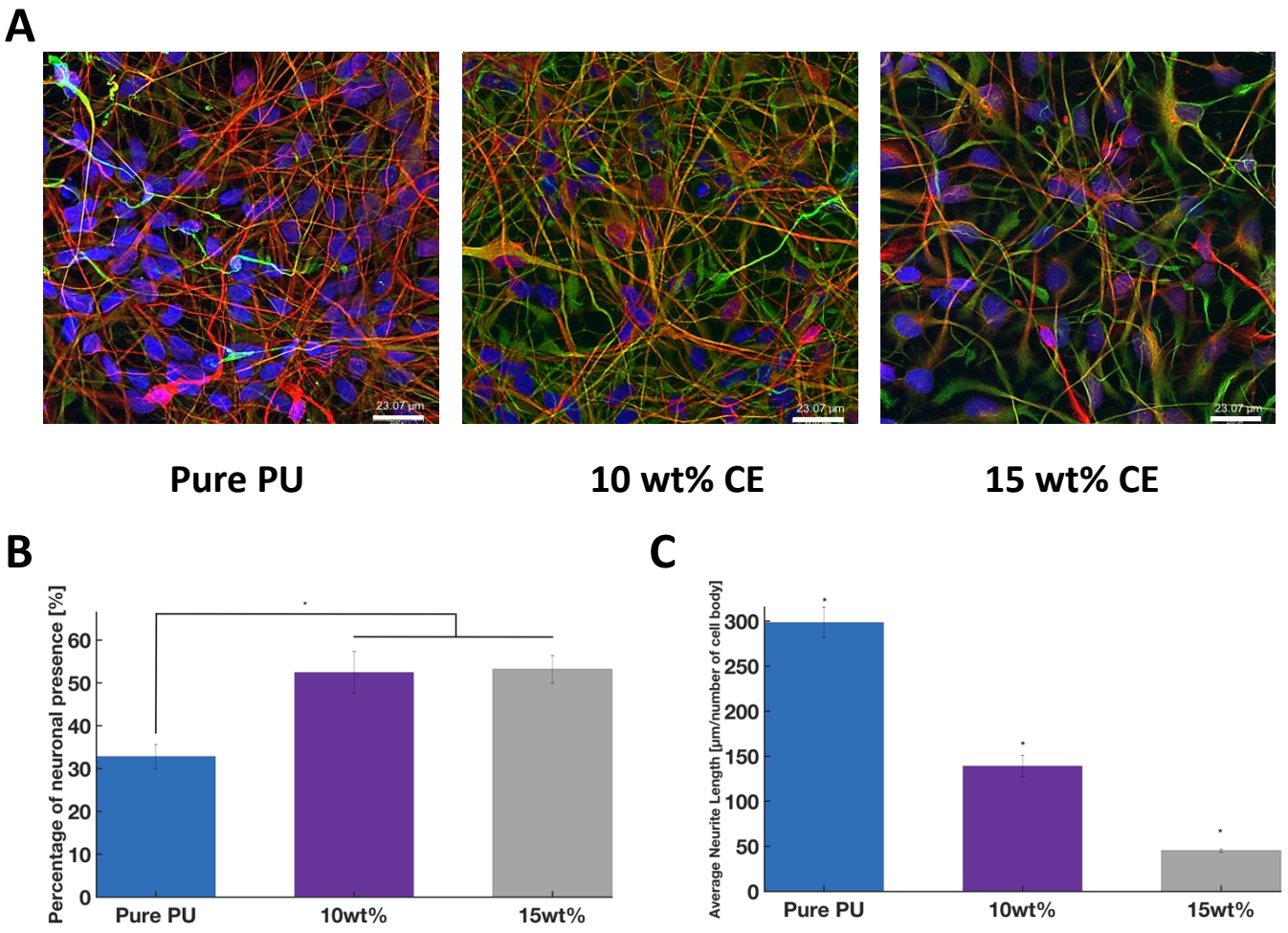

Fig. 6 Cytocompatibility of conductive elastomers A) Fluorescent images of ReNcell VM human neural precursor (ReN) cells grown on each of the experimental and control groups for seven days in culture. Neurons are visualized by anti β-tubulin III, in red, astrocyte cells by anti-GFAP, in green and nuclei are visualized by DAPI, in blue. Bar = 23.07 µm. Cell density (%) analysis of neuron presence on each of the experimental and control group is presented in B). An overall similar neuron coverage was observed on the conductive elastomers and a significant low neuronal survival was observed on control pure PU. Neural length analysis of the experimental and control group is presented in C) showed with significant ($p < 0.05$) longer neurite lengths the neurons grown on pure PU, followed by the 10 wt % CE composites. * Significant difference at $p < 0.05$

one might compare the neurite outgrowth response of the 10 wt% CE with the enhanced neurite extension seen on conventional rigid Pt electrodes *in vitro*[66], but with the real benefits of a fully polymeric material with mechanical flexibility for stretchable electronics. Additionally, while other studies developed PU-CPs composites with elastomeric properties and higher conductivities[23,27], they have not investigated the biological response of the material or application specific performance, which is of critical importance for implantable device applications. Overall, the obtained *in* vitro results within this study support that the CE sheets are cytocompatible, demonstrating their potential for use in implantable devices with further investigation. Future work will explore more in depth the biological response. While the cytocompatibility of the CE materials has been demonstrated here, it should be noted that in most applications such as the flexible array described below the majority of the neural tissue will be in contact with insulating elastomer such as PDMS which has long history of safe use in such applications.

Fabrication and characterisation of a CE electrode array

The 10 wt% and 15 wt% PEDOT:PSS CEs were fabricated into nine-electrode planar arrays using laser micromachining, as shown in Fig. 7 A - C. The delivery of biphasic stimulation was observed and the CIL for 0.2 ms phase width stimuli were captured (Fig. 8). The array fabricated from the 10 wt% PEDOT:PSS in PU had a significantly higher end of phase voltage (cathodic phase) than the array fabricated from the 15 wt% PEDOT:PSS in PU. The increased voltage in the biphasic transient is clearly a result of the increased access voltage, V_s. It is expected that this property is a function of the track length where the resistance of the CE system is strongly affected by loading. It is notable therefore that the voltage transient for the 15 wt% formulation was of similar amplitude in the charge

 This journal is © The Royal Society of Chemistry 20xx

Please do not adjust margins

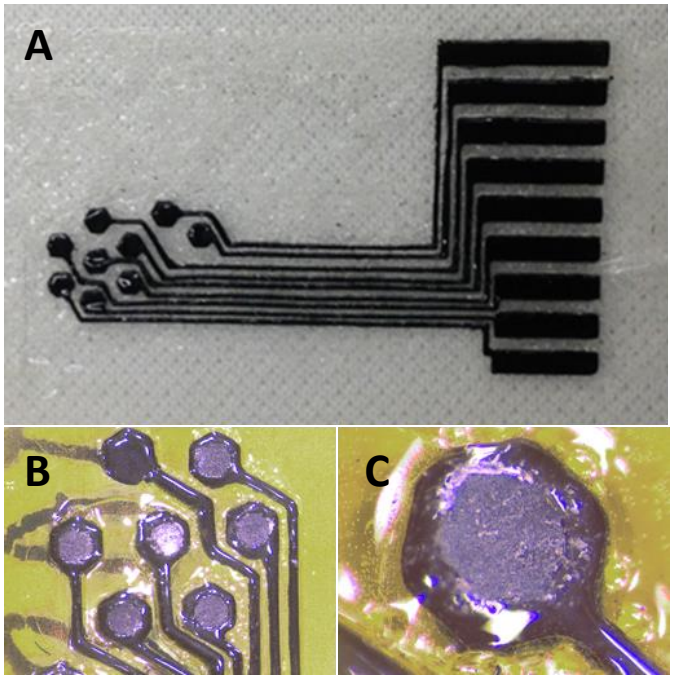

Fig. 7 CE array fabricated from 15 wt% PEDOT:PSS in PU for A. electrode sites, tracks and bond pads, embedded in PDMS matrices. B. shows opened electrode sites following laser ablation across array, and C. magnified image of single electrode site. Exposed area of electrode sites in all images is 900 µm in diameter.

injection phase to the Pt control electrodes. The square shape of the CE biphasic waveform suggests that the charge transfer has a resistive profile, similar to that of other CP based electrode modifications[67,68]. The electrochemical CIL of the electrodes produced from the 15 wt% PEDOT:PSS in PU were compared to Pt. The values obtained for the Pt were of the same scale and magnitude to those reported previously in the literature[42,43]. It was found that the CIL of the CE was significantly higher than that of the Pt. This is supported by the EIS and CV data shown in the material characterisation, where charge transfer to an electrolyte is substantially higher for the CE than the Pt (Fig.3). Ultimately, there is a trade-off between the system conductivity and charge injection properties of the electrodes.

Balancing these properties has enabled the development of a CE array with properties that are comparable to a Pt array of the same geometry. However, this suggests that the CE track length cannot be further increased in length or decreased in width without increasing the voltage profile and concurrently the power required to drive such an array. However, these results do validate the fabrication and function of a fully polymeric electrode array. The charge injection limit shows that the use of the CP component is very effective at transferring charge to the saline electrolyte. Future work will focus on quantifying the lifetime performance of such an array under both continuous stimulation and repeated mechanical strain. Methods to increase track conductivity while maintaining a fully polymeric array will also be explored.

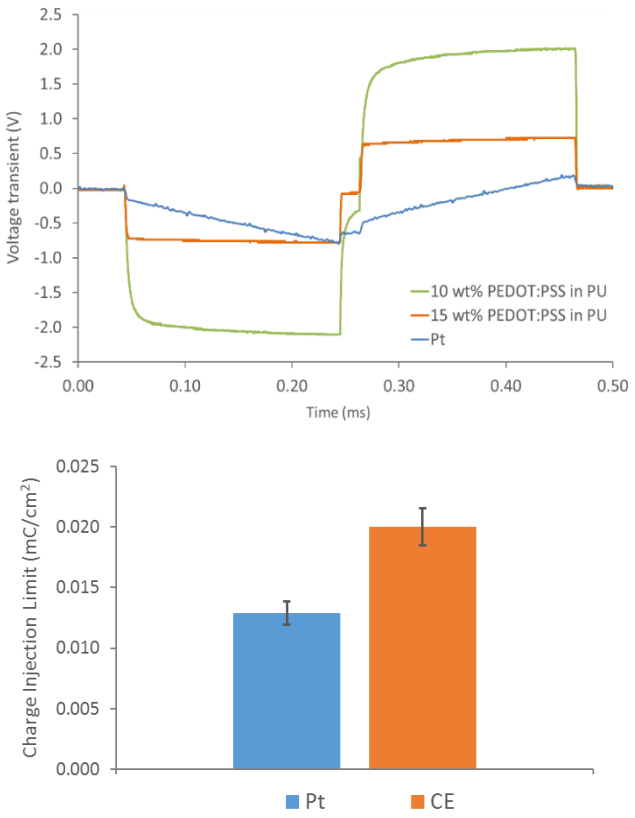

Fig. 8 CE array performance, with comparison of voltage transients between the arrays produced from 10 wt% and 15 wt% PEDOT:PSS in PU and Pt (top); and the electrochemical CIL of the array fabricated from 15 wt% PEDOT:PSS in PU (n=6) **(bottom)**

Conclusions

Solvent casting PEDOT:PSS dispersions in PU proved an effective way of fabricating electrically conductive elastomeric films. Increasing PEDOT:PSS loading generally acted to improve the electrochemical properties of CE films at the expense of mechanical robustness. Increasing PEDOT:PSS loadings resulted in the evolution of a connected PEDOT:PSS network within the PU matrix. A critical percolation threshold was found to occur between 5 - 10 wt%, with higher loadings exhibiting increased conductivity and charge storage capacity. CE films were found to have conductivities ranging from 0.25 to 6.6 $S.cm^{-1}$, placing them in the semiconductor range of conductivity. CE films were found to retain their elastomeric properties and UTS, although increased PEDOT content did result in increased Young's modulus and decreased strain at failure. Furthermore, the nano-rough morphology of the CEs induced a significant neuronal survival using ReNcell VM human neural precursor cell compared to pure PU matrix, while important changes in neurite outgrowth were associated with the mechanical stiffness of the composites.

The use of CEs allowed for the fabrication of a flexible, conformal microelectrode array. While charge injection via the

Please do not adjust margins

electrode into an electrolyte is quite efficient when compared to Pt controls, the delivery of stimulation was impacted by the reduced DC conductivity of the tracks. CEs with loading of 10 and 15 wt% PEDOT:PSS in PU were considered a suitable trade-off between electrical and mechanical properties. This technique involves a simple and straightforward process that is scalable for device manufacture. The resulting properties of the arrays emphasize the significant potential of CEs for next-generation flexible and stretchable electronics.

Conflicts of interest

There are no conflicts to declare.

Acknowledgements

The authors acknowledge funding from Healthcare Technologies Challenge Awards (HTCA) grant of the Engineering and Physical Sciences Research Council (EPSRC). The authors would like to thank Stephen Mow for his contributions in the development of laser machining processes.

References

1. Normann RA. Technology Insight: future neuroprosthetic therapies for disorders of the nervous system. *Nat Clin Pract Neurol*. 2007;3(8):444-452. doi:10.1038/ncpneuro0556
2. Shepherd R, Shivdasani M, biotechnology DN-… in, 2013 undefined. Visual prostheses for the blind. *Elsevier*. https://www.sciencedirect.com/science/article/pii/S0167779913001595. Accessed September 23, 2018.
3. Lee J, Kim D, Yoo S, Lee H, … GL-I, 2015 undefined. Emerging neural stimulation technologies for bladder dysfunctions. *ncbi.nlm.nih.gov*. https://www.ncbi.nlm.nih.gov/pmc/articles/PMC4386488/. Accessed September 28, 2018.
4. Cogan SF. Neural Stimulation and Recording Electrodes. *Annu Rev Biomed Eng*. 2008;10(1):275-309. doi:10.1146/annurev.bioeng.10.061807.160518
5. White RL, Gross TJ. An Evaluation of the Resistance to Electrolysis of Metals for Use in Biostimulation Microprobes. *IEEE Trans Biomed Eng*. 1974;BME-21(6):487-490. doi:10.1109/TBME.1974.324339
6. Woolley AJ, Desai HA, Steckbeck MA, Patel NK, Otto KJ. In situ characterization of the brain–microdevice interface using Device Capture Histology. *J Neurosci Methods*. 2011;201(1):67-77. doi:http://dx.doi.org/10.1016/j.jneumeth.2011.07.012
7. Polikov V, Tresco P, methods WR-J of neuroscience, 2005 undefined. Response of brain tissue to chronically implanted neural electrodes. *Elsevier*. https://www.sciencedirect.com/science/article/pii/S0165027005002931. Accessed September 23, 2018.
8. Cogan SF, Troyk PR, Ehrlich J, Plante TD. In Vitro Comparison of the Charge-Injection Limits of Activated Iridium Oxide (AIROF) and Platinum-Iridium Microelectrodes. *IEEE Trans Biomed Eng*. 2005;52(9):1612-1614. doi:10.1109/TBME.2005.851503
9. Amella AD, Patton AJ, Martens PJ, Lovell NH, Poole-Warren LA, Green RA. Freestanding, soft bioelectronics. In: *2015 7th International IEEE/EMBS Conference on Neural Engineering (NER)*. IEEE; 2015:607-610. doi:10.1109/NER.2015.7146696
10. Rivnay J, Owens RM, Malliaras GG. The Rise of Organic Bioelectronics. *Chem Mater*. 2014;26(1):679-685. doi:10.1021/cm4022003
11. Balint R, Cassidy N, biomaterialia SC-A, 2014 undefined. Conductive polymers: towards a smart biomaterial for tissue engineering. *Elsevier*. https://www.sciencedirect.com/science/article/pii/S1742706114000671. Accessed September 23, 2018.
12. Green R, Lovell N, Wallace G, Biomaterials LP-W-, 2008 undefined. Conducting polymers for neural interfaces: challenges in developing an effective long-term implant. *Elsevier*. https://www.sciencedirect.com/science/article/pii/S0142961208003220. Accessed September 23, 2018.
13. Poole-Warren L, Lovell N, Baek S, Green R. Development of bioactive conducting polymers for neural interfaces. *Expert Rev Med Devices*. 2010;7(1):35-49. doi:10.1586/erd.09.58
14. Yi N, Applications MA-BP for M, 2016 undefined. Conducting polymers and their biomedical applications. *Elsevier*. https://www.sciencedirect.com/science/article/pii/B9781782421054000109. Accessed September 23, 2018.
15. Hassarati RT, Goding JA, Baek S, Patton AJ, Poole-Warren LA, Green RA. Stiffness quantification of conductive polymers for bioelectrodes. *J Polym Sci Part B Polym Phys*. 2014;52(9):666-675. doi:10.1002/polb.23465
16. Baek S, Green RA, Poole-Warren LA. The biological and electrical trade-offs related to the thickness of conducting polymers for neural applications. *Acta Biomater*. 2014;10(7):3048-3058. doi:10.1016/j.actbio.2014.04.004
17. Kaur G, Adhikari R, Cass P, Bown M, Gunatillake P. Electrically conductive polymers and composites for biomedical applications. *RSC Adv*. 2015;5(47):37553-37567. doi:10.1039/C5RA01851J
18. Patton AJ, Poole-Warren LA, Green RA. Mechanisms for Imparting Conductivity to Nonconductive Polymeric Biomaterials. *Macromol Biosci*. 2016;16(8):1103-1121. doi:10.1002/mabi.201600057
19. Kim D-H, Abidian M, Martin DC. Conducting polymers grown in hydrogel scaffolds coated on neural prosthetic devices. *J Biomed Mater Res - Part A*. 2004;71(4):577-585.
20. Li P, Du D, Guo L, Guo Y, Ouyang J. Stretchable and conductive polymer films for high-performance electromagnetic interference shielding. *J Mater Chem C*.

 This journal is © The Royal Society of Chemistry 20xx

Please do not adjust margins

Please do not adjust margins

2016;4(27):6525-6532. doi:10.1039/C6TC01619G
21. Wang Y, Jing X. Intrinsically conducting polymers for electromagnetic interference shielding. *Polym Adv Technol*. 2005;16(4):344-351. doi:10.1002/pat.589
22. Choong C-L, Shim M-B, Lee B-S, et al. Highly Stretchable Resistive Pressure Sensors Using a Conductive Elastomeric Composite on a Micropyramid Array. *Adv Mater*. 2014;26(21):3451-3458. doi:10.1002/adma.201305182
23. Seyedin MZ, Razal JM, Innis PC, Wallace GG. Strain-Responsive Polyurethane/PEDOT:PSS Elastomeric Composite Fibers with High Electrical Conductivity. *Adv Funct Mater*. 2014;24(20):2957-2966. doi:10.1002/adfm.201303905
24. Pérez-Madrigal MM, Giannotti MI, Armelin E, Sanz F, Alemán C. Electronic, electric and electrochemical properties of bioactive nanomembranes made of polythiophene:thermoplastic polyurethane. *Polym Chem*. 2014;5(4):1248-1257. doi:10.1039/C3PY01313H
25. Sasaki M, Karikkineth BC, Nagamine K, Kaji H, Torimitsu K, Nishizawa M. Highly Conductive Stretchable and Biocompatible Electrode–Hydrogel Hybrids for Advanced Tissue Engineering. *Adv Healthc Mater*. 2014:n/a-n/a. doi:10.1002/adhm.201400209
26. Broda CR, Lee JY, Sirivisoot S, Schmidt CE, Harrison BS. A chemically polymerized electrically conducting composite of polypyrrole nanoparticles and polyurethane for tissue engineering. *J Biomed Mater Res A*. 2011;98(4):509-516. doi:10.1002/jbm.a.33128
27. Hansen TS, West K, Hassager O, Larsen NB. Highly Stretchable and Conductive Polymer Material Made from Poly(3,4-ethylenedioxythiophene) and Polyurethane Elastomers. *Adv Funct Mater*. 2007;17(16):3069-3073. doi:10.1002/adfm.200601243
28. Chen J, Dong R, Ge J, Guo B, Ma PX. Biocompatible, Biodegradable, and Electroactive Polyurethane-Urea Elastomers with Tunable Hydrophilicity for Skeletal Muscle Tissue Engineering. *ACS Appl Mater Interfaces*. 2015;7(51):28273-28285. doi:10.1021/acsami.5b10829
29. Khatoon H, Ahmad S. A review on conducting polymer reinforced polyurethane composites. *J Ind Eng Chem*. 2017;53:1-22. doi:10.1016/J.JIEC.2017.03.036
30. Robil?? G, Diaconu I, Buruian?? T, Buruian?? E, Coman P. Carboxylated polyurethane anionomers and their composites with polypyrrole. *J Appl Polym Sci*. 2000;75(11):1385-1392. doi:10.1002/(SICI)1097-4628(20000314)75:11<1385::AID-APP10>3.0.CO;2-Q
31. Deligöz H, Tieke B. Conducting Composites of Polyurethane Resin and Polypyrrole: Solvent-Free Preparation, Electrical, and Mechanical Properties. *Macromol Mater Eng*. 2006;291(7):793-801. doi:10.1002/mame.200600126
32. Çakmak G, Küçükyavuz Z, Küçükyavuz S. Flexible and conducting composites of polypyrrole and polydimethylsiloxane. *J Appl Polym Sci*. 2004;93(2):736-741. doi:10.1002/app.20536
33. Ustamehmetoğlu B, Kızılcan N, Demir Ö. Electrocopolymerization of pyrrole with bis(4-aminobutyl)polydimethylsiloxane. *Pigment Resin Technol*. 2012;41(3):179-186. doi:10.1108/03699421211226471
34. Kızılcan N, Öz NK, Ustamehmetoğlu B, Akar A. High conductive copolymers of polypyrrole-α,ω-diamine polydimethylsiloxane. *Eur Polym J*. 2006;42(10):2361-2368. doi:10.1016/J.EURPOLYMJ.2006.05.016
35. Abbasi F, Mirzadeh H, Katbab A-A. Modification of polysiloxane polymers for biomedical applications: a review. *Polym Int*. 2001;50(12):1279-1287. doi:10.1002/pi.783
36. Lamba NMK, Woodhouse KA, Cooper SL, Lelah MD. *Polyurethanes in Biomedical Applications*. CRC Press; 1998.
37. Harper CA. *Handbook of Plastics, Elastomers, and Composites*. McGraw-Hill; 2002. https://www.accessengineeringlibrary.com/browse/handbook-of-plastics-elastomers-and-composites-fourth-edition. Accessed September 22, 2018.
38. Kumar, Santosh and Singh RN. *Modelling of Magmatic and Allied Processes*. (Springer, ed.).; 2014.
39. Vallejo-Giraldo C, Krukiewicz K, Calaresu I, et al. Attenuated Glial Reactivity on Topographically Functionalized Poly(3,4-Ethylenedioxythiophene):P-Toluene Sulfonate (PEDOT:PTS) Neuroelectrodes Fabricated by Microimprint Lithography. *Small*. 2018;14(28):1800863. doi:10.1002/smll.201800863
40. O'Keeffe GW, Dockery P, Sullivan AM. Effects of growth/differentiation factor 5 on the survival and morphology of embryonic rat midbrain dopaminergic neurones in vitro. *J Neurocytol*. 2004;33(5):479-488. doi:10.1007/s11068-004-0511-y
41. Schuettler M, Stiess S, King B, Suaning GJ. Fabrication of implantable microelectrode arrays by laser-cutting of silicone rubber and platinum foil. *J Neural Eng*. 2005;(2):121-128.
42. Green RA, Toor H, Dodds C, Lovell NH. Variation in performance of platinum electrodes with size and surface roughness. *Sensors Mater*. 2012;24(4).
43. Green RA, Matteucci PB, Dodds CWD, et al. Laser patterning of platinum electrodes for safe neurostimulation. *J Neural Eng*. 2014;11(5). doi:10.1088/1741-2560/11/5/056017
44. Dodds CWD, Wong YT, Byrnes-Preston PJ, Rendl M, Lovell NH, Suaning GJ. Performance of Laser Fabricated Stimulating Electrode Arrays for a Retinal Prosthesis in Saline. In: *Proceedings of the 4th International IEEE EMBS Conference on Neural Engineering*. Antalya, Turkey; 2009:88-91.
45. Cogan SF, Garrett DJ, Green RA. Electrochemical Principles of Safe Charge Injection. In: *Neurobionics: The Biomedical Engineering of Neural Prostheses*. ; 2016:55-88. doi:10.1002/9781118816028.ch3
46. Kim YH, Sachse C, MacHala ML, May C, Müller-Meskamp L, Leo K. Highly conductive PEDOT:PSS electrode with optimized solvent and thermal post-treatment for ITO-free organic solar cells. *Adv Funct Mater*. 2011.

Please do not adjust margins

Please do not adjust margins

doi:10.1002/adfm.201002290
47. Drobny JG. *Handbook of Thermoplastic Elastomers*. William Andrew Pub; 2007.
48. Someya T, Bao Z, Malliaras GG. The rise of plastic bioelectronics. *Nature*. 2016;540(7633):379-385. doi:10.1038/nature21004
49. Roland CM. Chapter 02163 - Reinforcement of Elastomers. 2015. doi:10.1016/B978-0-12-803581-8.02163-9
50. Fröhlich J, Niedermeier W, Luginsland H-D. The effect of filler-filler and filler-elastomer interaction on rubber reinforcement. doi:10.1016/j.compositesa.2004.10.004
51. Voet A. Reinforcement of elastomers by fillers: Review of period 1967–1976. *J Polym Sci Macromol Rev*. 1980;15(1):327-373. doi:10.1002/pol.1980.230150107
52. Vallejo-Giraldo C, Pampaloni NP, Pallipurath AR, et al. Preparation of Cytocompatible ITO Neuroelectrodes with Enhanced Electrochemical Characteristics Using a Facile Anodic Oxidation Process. *Adv Funct Mater*. 2018;28(12):1605035. doi:10.1002/adfm.201605035
53. Levitan I, Kaczmarek L. The neuron: cell and molecular biology. 2015. https://books.google.ch/books?hl=fr&lr=&id=t4V2CAAAQBAJ&oi=fnd&pg=PP1&dq=I.+B.+Levitan+and+L.+K.+Kaczmarek,+The+neuron:+cell+and+molecular+biology,+Oxford+University+Press,+USA,+2015.&ots=8LtzBQusJx&sig=2bjYsTocNsFZQeuLpH29rmqdd0Q. Accessed September 29, 2018.
54. Escuin S, Neuritogenesis EG-L-M for, 2007 undefined. Adhesion-induced intracellular mechanisms of neurite elongation. *Springer*. https://link.springer.com/content/pdf/10.1007/978-0-387-68561-8_1.pdf. Accessed September 29, 2018.
55. Marín O, Valiente M, … XG-CSH, 2010 undefined. Guiding neuronal cell migrations. *cshperspectives.cshlp.org*. http://cshperspectives.cshlp.org/content/early/2010/01/11/cshperspect.a001834.abstract. Accessed September 29, 2018.
56. Brunetti V, Maiorano G, Rizzello L, et al. Neurons sense nanoscale roughness with nanometer sensitivity. *Proc Natl Acad Sci U S A*. 2010;107(14):6264-6269. doi:10.1073/pnas.0914456107
57. Blumenthal N, … OH-P of the, 2014 undefined. Stochastic nanoroughness modulates neuron–astrocyte interactions and function via mechanosensing cation channels. *Natl Acad Sci*. http://www.pnas.org/content/111/45/16124.short. Accessed September 29, 2018.
58. Jiang FX, Yurke B, Schloss RS, Firestein BL, Langrana NA. Effect of Dynamic Stiffness of the Substrates on Neurite Outgrowth by Using a DNA-Crosslinked Hydrogel. *Tissue Eng Part A*. 2010;16(6):1873-1889. doi:10.1089/ten.tea.2009.0574
59. Discher D, Janmey P, Science YW-, 2005 undefined. Tissue cells feel and respond to the stiffness of their substrate. *science.sciencemag.org*. http://science.sciencemag.org/content/310/5751/1139.short?casa_token=UgbUZmS7eVEAAAAA:wVhhBMsZjq3ZV2gImEkUsN0MtqHXTgZcWL4-EHxnl6GzAOwxtZzvd47Kh8VD1AmLxzwtg7Z1P65PGw. Accessed September 29, 2018.
60. Solon J, Levental I, Sengupta K, journal PG-B, 2007 undefined. Fibroblast adaptation and stiffness matching to soft elastic substrates. *Elsevier*. https://www.sciencedirect.com/science/article/pii/S00634950771696X. Accessed September 29, 2018.
61. Chicurel M, Chen C, biology DI-C opinion in cell, 1998 undefined. Cellular control lies in the balance of forces. *Elsevier*. https://www.sciencedirect.com/science/article/pii/S095567498801452. Accessed September 29, 2018.
62. Tuft BW, Zhang L, Xu L, et al. Material Stiffness Effects on Neurite Alignment to Photopolymerized Micropatterns. *Biomacromolecules*. 2014;15(10):3717-3727. doi:10.1021/bm501019s
63. Heidemann S, neurobiology RB-C opinion in, 1991 undefined. Growth cone motility. *Elsevier*. https://www.sciencedirect.com/science/article/pii/095943889190050H. Accessed September 29, 2018.
64. Fischer T, Steinmetz P, engineering DO-A of biomedical, 2005 undefined. Robust micromechanical neurite elicitation in synapse-competent neurons via magnetic bead force application. *Springer*. https://idp.springer.com/authorize/casa?redirect_uri=https://link.springer.com/article/10.1007/s10439-005-5509-1&casa_token=j51X2mVbxMsAAAAA:zuIAZJIyUUT4C3ZMqbPu0M3Es1bMvdjSrg0GpEdwaFoQ3mT7BpRrL7XaRpAlDD7thgvz1Tz3bQrCOWfY. Accessed September 29, 2018.
65. Zheng J, Lamoureux P, Santiago V, Dennerll T, Buxbaum RE, Heidemann SR. Tensile regulation of axonal elongation and initiation. *J Neurosci*. 1991;11(4):1117-1125. doi:10.1523/JNEUROSCI.11-04-01117.1991
66. Vallejo-Giraldo C, Krukiewicz K, Calaresu I, et al. Attenuated Glial Reactivity on Topographically Functionalized Poly(3,4-Ethylenedioxythiophene):P-Toluene Sulfonate (PEDOT:PTS) Neuroelectrodes Fabricated by Microimprint Lithography. *Small*. 2018;14(28):1800863. doi:10.1002/smll.201800863
67. Green RA, Matteucci PB, Hassarati RT, et al. Performance of conducting polymer electrodes for stimulating neuroprosthetics. *J Neural Eng*. 2013;10(1). doi:10.1088/1741-2560/10/1/016009
68. Hassarati RT, Dueck WF, Tasche C, Carter PM, Poole-Warren LA, Green RA. Improving Cochlear Implant Properties Through Conductive Hydrogel Coatings. *IEEE Trans Neural Syst Rehabil Eng*. 2014;22(2):411-418. doi:10.1109/TNSRE.2014.2304559

 This journal is © The Royal Society of Chemistry 20xx

Please do not adjust margins